IGF26 - 26th International Conference on Fracture and Structural Integrity

Single overloads FCG modeling considering damage accumulation

E.R. Sérgio[a*], M.F. Borges[a], D.M. Neto[a], F.V. Antunes[a], J.P. Pais[a]

[a]Univ. Coimbra, Centre for Mechanical Engineering, Materials and Processes (CEMMPRE), Department of Mechanical Engineering;
edmundo.sergio@uc.pt ; micaelfriasborges@outlook.pt; diogo.neto@dem.uc.pt; *Correspondence: edmundo.sergio@uc.pt.: +351 790700 (F.A.)

Abstract

In this study, Fatigue Crack Growth (FCG) in a CT specimen, submitted to single overloads, is predicted by a node release numerical model, which considers the plastic strain to be the main FCG driving force. The Gauss-Tvergaard-Needleman (GTN) damage model was implemented to account for the, inevitable, growth and nucleation of microvoids in the occurrence of high levels of plastic strain. Crack closure shown to be a crucial mechanism influencing the differences between both models, as well as it explains the effects of the overloads on the FCG rate.

Keywords: Type your keywords here, separated by semicolons ;

Introduction

Components in real engineering applications are usually submitted to complex loading patterns, being common the occurrence of variable amplitude loading situations. The stress intensity factor range (ΔK), which is widely considered as the FCG driving force, is not able to explain the FCG process when these loading conditions occur. The appearance of the crack closure concept [1] allowed to explain the trends observed experimentally in variable amplitude loading conditions [2]–[4]. Moreover, the contact of the crack flanks have been observed experimentally [5], [6]. This contact is supposed to occurs due to different mechanisms, which cause distinct types of crack closure, namely: Plastic-induced crack closure (PICC), Oxide-induced crack closure (OICC) and Roughness-induced crack closure (RICC) [7].

---

* Corresponding author. Tel.: +351 790700;
  E-mail address: fernando.ventura@dem.uc.pt

A numerical model, which assume the cyclic plastic deformation at the crack-tip to be the FCG driving force, has been used to predict the Fatigue Crack Growth Rate (FCGR) under constant loading [8] and variable amplitude loading [9] situations. On both cases the crack closure phenomenon was found to have a key effect on FCGR.

The occurrence of high levels of plastic strain is linked to the accumulation of damage, which occurs due to the processes of growth, nucleation and coalescence of micro-voids [10]. The damage evolution is usually accessed through damage models [11], as is the case of the GTN model. The introduction of the damage component, which affects the materials behavior [12], on the aforementioned numerical model, proved to affect the crack closure level and therefore *da/dN* [13]. As crack closure was found to be responsible for the effect of overloads on FCG rate behaviour [14] it is expected that the inclusion of the damage, caused by the processes involving microvoids, will influence *da/dN* in this loading case. Thus, this study pretends to evaluate the influence of the GTN model, on FCG, in Compact Tension (CT) specimens subjected to single overloads.

2.Numerical Model

All the numerical simulations were performed with the in-house finite element code DD3IMP, originally developed to numerical simulate sheet metal forming processes [15][16]. The mechanical model follows an updated lagrangian scheme to describe the evolution of the deformation process, which considers large elastoplastic strains and rotations.

2.1. Material Constitutive Model

The study was conducted on a AA6082-T6 aluminium alloy. Hooke's law was used to describe the isotropic elastic behaviour of the material. The yield surface was described through the von Mises yield criterion. The hardening behaviour was defined by Voce law, given by equation 1.

$$\sigma_y = Y_0 + (Y_{Sat} - Y_0)[1 - exp(-C_Y \bar{\varepsilon}^p)] \tag{1}$$

where Y_0 is the yield stress, Y_{Sat} is the isotropic saturation stress, C_Y is a parameter of the Voce law that gives information as the isotropic saturation stress is reached more or less rapidly and $\bar{\varepsilon}^p$ is the equivalent plastic strain. The non-linear kinematic hardening was predicted by the Armstrong-Frederick law, which can be written as:

$$\dot{\boldsymbol{X}} = C_X \left[\frac{X_{sat}}{\bar{\sigma}} (\boldsymbol{\sigma}' - \boldsymbol{X}) \right] \dot{\bar{\varepsilon}}^p \quad with \, \dot{\boldsymbol{X}}(0) = \boldsymbol{0}, \tag{2}$$

where $\boldsymbol{X}$ is the back stress tensor, X_{Sat} and C_x are material parameters, **σ'** is the deviatoric component of the Cauchy stress tensor, and $\bar{\sigma}$ is the equivalent stress. The parameters for both laws, together with the respective elastic properties, are presented in Table 1.

Table 1. Swift and Armstrong-Frederick parameters and elastic properties for the aluminium alloy AA 6082-TX

Material	E (GPa)	ν (-)	Y_0 (MPa)	k (MPa)	n (-)	X_{Sat} (MPa)	C_X (-)
AA6082-T6	72.26	0.29	288.96	389.00	0.056	111.84	138.80

The GTN damage model yield potential, given by equation 3, considers the void volume fraction as a parameter and accounts to the resistance loss, due to the occurrence of voids that can grow by the plastic deformation, of the material matrix [17].

$$\phi = \left(\frac{\bar{\sigma}^2}{\sigma_y}\right)^2 + 2q_1 f \, cosh \left(q_2 \frac{tr \, \boldsymbol{\sigma}}{2\sigma_y}\right) - 1 - q_3 f^2 \tag{3}$$

where $\boldsymbol{\sigma}$ is the stress tensor, q_1, q_2 and q_3 the Tvergaard void interaction parameters, f the void volume fraction, p the hydrostatic pressure and σ_y the flow stress in the matrix material which is defined in terms of the effective plastic

strain, using the Voce law (equation 1). The evolution of porosity, $\dot{f}$, which in this study is considered to occur only due to the nucleation and growth of micro-voids, is given by equation 4.

$$\dot{f} = (f - f^2)\dot{\gamma}\sigma_y \sinh\left(\frac{3p}{2\sigma_y}\right) + \frac{f_N}{s_N\sqrt{2\pi}} exp\left[-\frac{1}{2}\left(\frac{\bar{\varepsilon}^n - \varepsilon_N}{s_N}\right)^2\right]\dot{\bar{\varepsilon}}^p \qquad (4)$$

where $\dot{\gamma}$ is the plastic multiplier, ε_N is the mean plastic strain of the Gaussian distribution, used to describe the nucleation process, which considers a standard deviation s_N, and a maximum nucleation amplitude f_N. The material parameters of the GTN model were based on the existing literature [18] for the AA6082-T6 aluminium alloys and are presented on Tab. 2. Note that the coalescence process is deactivated.

Table 2. Parameters for the GTN model. Nucleation is driven only by plastic strain and the coalescence process is deactivated.

Material	ε_N	s_N	f_N	q_1	q_2	q_3	f_0
AA 6082-T6	0.3	0.1	0.05	1.5	1	2.25	0.00035

2.2. Finite element model and loading case

This study models a CT specimen, in accordance to ASTM E647 [[19]] standard, which is subjected to mode I cyclic loading. The geometry of the deformable body is presented in Fig. 1a. Plane strain conditions were assumed by constraining out of plane displacements on a both faces of the component, as shown in Fig. 2b. Due to the existent symmetry, only half of the specimen is modelled.
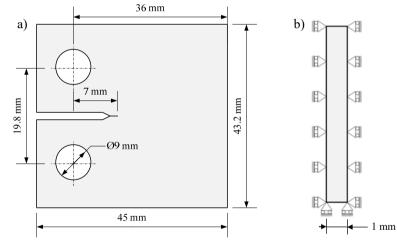

Figure 1. (a) CT specimen dimensions, the thickness is of 6 mm; (b) Plane stress boundary conditions. Adapted from [14].

The specimen was meshed with 8-node hexahedral finite elements, a selective reduced integration technique was adopted to avoid volumetric locking [20]. To capture the stress and strain gradients which occur near the crack tip, relatively refined elements (size of 8 μm) were assigned to this zone, in the crack growth direction [21]. To reduce the computational cost only one single layer of elements was used in the thickness direction and, also, the specimen received a coarser mesh on the zones apart from the crack propagation zone, as shown in Fig.2.
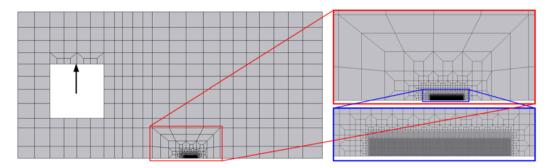
Figure 2. Finite element mesh. The refined mesh is shown in the image on the bottom left corner.

The specimen was submitted to a constant amplitude triangular load varying between F_{min}=8 N and F_{max}=80 N, resulting in a stress ratio, $R=0.1$. After 3300 loading cycles an F_{ol}=114N overload is applied, being followed by 5700 load cycles with the base load. This way, the overload is applied when the propagation is already stable, as crack closure is already fully induced. This mechanism is of major importance when concerning overloads as it is able to explain the transient crack growth behaviour after an overload [22]. The contact of the crack flanks is modelled with a rigid plane aligned with the crack symmetry plane. This mechanism may be deactivated, numerically, by disabling the contact of the nodes that cover the crack flanks.

The overload ratio (OLR) was defined through equation 5 [22]:

$$OLR = \frac{F_{OL} - F_{min}}{F_{max} - F_{min}} = \frac{\Delta F_{OL}}{\Delta F_{BL}}$$

(4)

where F_{max}, F_{min}, and F_{OL} are the maximum baseline, minimum baseline, and peak loads, respectively. Thus, the applied overload results in an *OLR*=1.368.

2.3. Crack propagation scheme

As referred the FCG process is modelled through a node release strategy [14], [23], [24] by successive debonding of the current crack front nodes. The crack increments occur always at minimum load to avoid convergence problems related to crack propagation at maximum load. Each crack increment corresponds to one finite element that, at the crack tip zone, has a size of 8 μm. [8]. Crack propagation occurs when the plastic strain, measured at the Gauss points and averaged at the node containing the crack tip reaches a critical value, ε_c^p. This parameter is supposed to be a material property and, based on prior studies it was considered to be 261%. Thus, the FCG rate is computed by the ratio between each crack increment and the total number of load cycles required to reach the critical plastic strain. A Total Plastic Strain (TPS) approach is followed, this way, the plastic strain, and porosity, accumulated in the previous load cycles, in a certain node are not reset at each propagation.

3. Results

Fig. 3a shows the evolution of *da/dN* in terms of the crack growth. Note that the *x*-axis presents the crack size in relation to the one verified at the instant of the overload application, thus the negative and positive values of a-a_{OL} represent the crack size before and after the overload application, respectively. Before the overload application, at constant amplitude loading, the model with GTN presents a slighter faster propagation rate, this way, the overload is applied at a higher crack size (15.296 mm) in comparison with the model without GTN (15.216 mm). Also, while the last presents a stable propagation since the beginning, as *da/dN* is almost constant, the model with GTN suffers a transient behavior. There is an initial peak in *da/dN*, at the first propagations, followed by a fast decrease on the propagation rate until the steady propagation zone is reached. This occurs due to the stabilization of cyclic plastic deformation and formation of residual plastic wakes [24]. When the overload is applied, *da/dN* reaches another peak

in the model with GTN, as the overload application causes an increase on the plastic strain accumulation at the crack tip. On the other hand, the model without GTN shows a smaller increase in the propagation speed. This occurs because the overload is applied during an ongoing propagation. Thus, the cumulative plastic deformation is already close to the critical value and the increment in plastic deformation, caused by the overload, saves only a few load cycles, compared to the ones needed if constant amplitude was kept, resulting in the, verified, small increase in *da/dN*. At constant amplitude loading, following the overload, there is a progressive reduction on *da/dN* with crack increments, on both versions of the model, showing the effect of load history. Also, both models present delayed retardation as a minimum in *da/dN* is reached. However, the reduction in the model without GTN is smaller, because no peak occurred on the overload, but more abrupt as the minimum propagation rate is reached sooner. The subsequent load cycles cause the crack to grow inside the plastic zone, produced by the overload, causing *da/dN* to increase. Here, there is an initial faster increase in the model without GTN, followed by a stabilization at a lower crack growth rate, in comparison with the model with GTN, as highlighted by the dashed lines. Moreover, even if the stabilization after the minimum in *da/dN* is faster for this model, it requires more load cycles from the overload application instant. In the stable propagation zone, after the overload, the model with GTN presents a slightly higher *da/dN* than the model without GTN.

Fig. 3b presents the evolution of the crack size in terms of the applied load cycles, analogously to Fig. 3a the *x*-axis presents the load cycles relatively to the instant of the overload application (3300th load cycle). As expected, before the overload, the slope of the curve of the model considering GTN is higher. In both models, immediately after the overload there is a reduction in the increase rate of *a*. Also, when the stable propagation zone is once again reached, the slope of the curves (highlighted by the full lines) is very similar to the one that was verified initially (shown by the dotted line), i.e., before the overload. This occurs because, once the crack grows outside the plastic zone induced by the overload, its effect ceases.
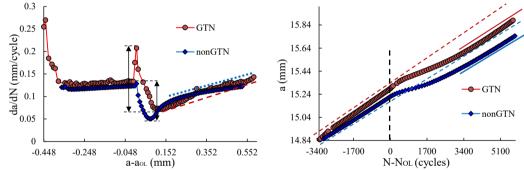

Figure 3. **(a)** *da/dN* in terms of the crack size, in relation to the one verified at the overload application, for both versions of the model. **(b)** Evolution of the crack size in terms of the applied load cycles, again in relation to the overload application cycle (3300th).

In previous studies [13] crack closure shown to be able to explain the differences between both versions of the model. Thus, it was evaluated, on the last load cycle before each propagation, at the node immediately behind the crack tip, through the following parameter:

$$U^* = \frac{F_{open} - F_{min}}{F_{max} - F_{min}} \times 100$$

(5)

where U* is the crack closure level and F_{open} is the opening load.

Fig. 4 shows the crack closure evolution through the loading cycles, *x*-axis is presented in an analogous way as it appears in Fig 3a. In the case of the model considering GTN, the crack closure rises at the first propagations, which is in accordance with the reduction of *da/dN* presented in Fig. 3a. This occurs because, at the first loading cycles, the material is virgin in terms of plastic deformation. The successive propagations cause the formation of plastic wakes, at the crack flanks, inducing PICC. Once the crack closure stabilizes, the same occurs with *da/dN*. In the case of the model without GTN, crack closure is not present in the last load cycles of the propagations before the overload. This

does not mean that crack closure does not exists as it is present, on the initial load cycles, after each propagation. However, due to the occurrence of strain ratcheting it ceases with the accumulation of the load cycles – during each propagation. Thus, the overall crack closure level is little, explaining the absence of the initial transient behaviour in *da/dN,* as occurs in the model with GTN. When the overload is applied, crack closure drops in the model with GTN due to crack tip blunting. This phenomenon disables the contact of the crack flanks and consequentially crack closure which explains the increase in *da/dN*. On the other hand, the model without GTN suffers an increase in the overall crack closure level immediately after the overload, as proven by the occurrence of crack closure in the last load cycle. As referred the overload is applied during an ongoing propagation, thus, once the crack propagates the crack tip blunting may be removed by the resharpening of the crack. Then, the higher levels of plastic strain caused by the overload may well induce higher levels of crack closure. Thus, even if the higher plastic strain would tend to cause higher crack growth rates, the also higher level of crack closure balances the *da/dN* trend. After the overload application crack closure rises, explaining the minimum achieved in *da/dN* in both models. The successive propagations, after the overload, cause the crack closure to drop, as the crack grows outside the intense plastic zone caused by the overload. This drop in crack closure result in an increase in *da/dN* in both models. The more prominent drop in crack closure in the model without GTN, as it returns to ceases in the last load cycles, causes a higher increase in *da/dN* in comparison with the model with GTN. Moreover, as the level of crack closure in the model with GTN takes time to stabilize, into the values verified before the overload, and the model with GTN returns abruptly to these values, the slightly higher *da/dN* in the stable propagation zone, after de overload, in the model with GTN is explained.
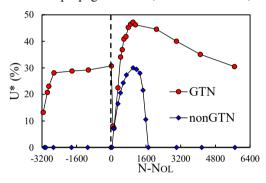

Figure 4. Crack closure evolution, for both versions of the model, in terms of the of the applied load cycles, again in relation to the overload application cycle, for both versions of the model.

4.Conclusions

Fatigue crack growth, in the occurrence of single overloads, is predicted assuming cyclic plastic deformation at the crack tip to be the main damage mechanism. The growth and nucleation of microvoids accounts for the damage accumulation due to the plastic strain build-up. The main conclusions are:

- In this material, the introduction of the GTN model causes a transient behavior at the first propagation, which is explained by the crack closure stabilization. This does not occur in the model without GTN, as strain ratcheting causes the crack closure to cease on the last load cycles, resulting in low overall crack closure levels.
- The inexistence of crack closure in the model without GTN compensates the higher plastic strains at the crack tip, that previous studies shown to typically occurs with the introduction of GTN, leveling the *da/dN* between both models.
- The increase in crack closure in the model without GTN, due to the overload application, causes a higher decrease of *da/dN,* in the propagations afterward the overload, in comparison to the model with GTN.
- The crack closure abruptly ceases again, some propagations after the overload, in the model without GTN, causing an higher increase in *da/dN* in this model after the minimum in the propagation rate is reached.
- As crack closure takes more time to stabilize into the levels prior to the overload application, in comparison to the model without GTN were it returns to cease suddenly, an higher *da/dN* in the second

stable propagation zone is verified.

Acknowledgements

References

[1]   W. Elber, "The Significance of Fatigue Crack Closure," in *Damage Tolerance in Aircraft Structures*, M. S. Rosenfeld, Ed. West Conshohocken, PA: ASTM International, 1971, pp. 230–242.

[2]   L. F. P. Borrego, J. D. Costa, and J. A. M. Ferreira, "Plasticity induced closure under variable amplitude loading in AlMgSi aluminum alloys," *Procedia Struct. Integr.*, vol. 5, pp. 85–92, 2017, doi: https://doi.org/10.1016/j.prostr.2017.07.072.

[3]   A. U. de Koning, "A Simple Crack Closure Model for Prediction of Fatigue Crack Growth Rates Under Variable-Amplitude Loading," in *Fracture Mechanics*, R. Roberts, Ed. West Conshohocken, PA: ASTM International, 1981, pp. 63–85.

[4]   O. Keui and O. Kiyotsugu, "FEM analysis of crack closure and delay effect in fatigue crack growth under variable amplitude loading," *Eng. Fract. Mech.*, vol. 9, no. 2, pp. 471–480, 1977, doi: https://doi.org/10.1016/0013-7944(77)90039-X.

[5]   P. LOPEZ-CRESPO *et al.*, "Overload effects on fatigue crack-tip fields under plane stress conditions: surface and bulk analysis," *Fatigue Fract. Eng. Mater. Struct.*, vol. 36, no. 1, pp. 75–84, Jan. 2013, doi: https://doi.org/10.1111/j.1460-2695.2012.01670.x.

[6]   A. Steuwer, J. Santisteban, M. Turski, P. Withers, and T. Buslaps, "High-Resolution Strain Mapping in Bulk Samples Using Full-Profile Analysis of Energy-Dispersive Synchrotron X-Ray Diffraction Data," *J. Appl. Crystallogr.*, vol. 37, 2005, doi: 10.1016/j.nimb.2005.06.049.

[7]   R. Pippan and A. Hohenwarter, "Fatigue crack closure: a review of the physical phenomena," *Fatigue Fract. Eng. Mater. Struct.*, vol. 40, no. 4, pp. 471–495, Apr. 2017, doi: 10.1111/ffe.12578.

[8]   M. Borges, D. M. Neto, and F. V Antunes, "Numerical simulation of fatigue crack growth based on accumulated plastic strain," *Theor. Appl. Fract. Mech.*, vol. 108, p. 102676, 2020, doi: 10.1016/j.tafmec.2020.102676.

[9]   R. S. D.M. Neto, M.F. Borges, F.V. Antunes, "Numerical analysis of Super Block 2020 loading sequence," *Eng. Fract. Mech.*, 2020.

[10]   G. Rousselier, "Ductile fracture models and their potential in local approach of fracture," *Nucl. Eng. Des.*, vol. 105, no. 1, pp. 97–111, 1987, doi: https://doi.org/10.1016/0029-5493(87)90234-2.

[11]   J.-J. Marigo, C. Maurini, and K. Pham, "An overview of the modelling of fracture by gradient damage models," *Meccanica*, vol. 51, no. 12, pp. 3107–3128, 2016, doi: 10.1007/s11012-016-0538-4.

[12]   J. Lemaitre, "Phenomenological Aspects of Damage," in *A Course on Damage Mechanics*, Berlin, Heidelberg: Springer Berlin Heidelberg, 1996, pp. 1–37.

[13]   E. R. Sérgio, F. V Antunes, M. F. Borges, and D. M. Neto, "FCG modelling considering the combined effects of cyclic plastic deformation and growth of micro-voids," *Materials (Basel).*, pp. 1–18, 2021.

[14]   D. M. Neto, M. F. Borges, F. V Antunes, and J. Jesus, "Mechanisms of fatigue crack growth in Ti-6Al-4V alloy subjected to single overloads," *Theor. Appl. Fract. Mech.*, vol. 114, p. 103024, 2021, doi: https://doi.org/10.1016/j.tafmec.2021.103024.

[15]   M. C. Oliveira, J. L. Alves, and L. F. Menezes, "Algorithms and Strategies for Treatment of Large Deformation Frictional Contact in the Numerical Simulation of Deep Drawing Process," *Arch. Comput. Methods Eng.*, vol. 15, no. 2, pp. 113–162, 2008, doi: 10.1007/s11831-008-9018-x.

[16]   L. F. Menezes and C. Teodosiu, "Three-dimensional numerical simulation of the deep-drawing process using solid finite elements," *J. Mater. Process. Technol.*, vol. 97, no. 1, pp. 100–106, 2000, doi: https://doi.org/10.1016/S0924-0136(99)00345-3.

[17]   A. Bourih, W. Kaddouri, T. Kanit, S. Madani, and A. Imad, "Effective yield surface of porous media with random overlapping identical spherical voids," *J. Mater. Res. Technol.*, vol. 7, no. 2, pp. 103–117, 2018, doi: https://doi.org/10.1016/j.jmrt.2017.01.002.

[18]   A. Kami, B. M. Dariani, A. Sadough Vanini, D. S. Comsa, and D. Banabic, "Numerical determination of the forming limit curves of anisotropic sheet metals using GTN damage model," *J. Mater. Process. Technol.*, vol. 216, pp. 472–483, 2015, doi: https://doi.org/10.1016/j.jmatprotec.2014.10.017.

[19]   ASTM E 647-11: Standard test method for measurement of fatigue crack growth rates. Philadelphia: American Society for Testing and Materials, 2011, ASTM

[20]   T. J. R. Hughes, "Generalization of selective integration procedures to anisotropic and nonlinear media," *Int. J. Numer. Methods Eng.*, vol. 15, no. 9, pp. 1413–1418, Sep. 1980, doi: https://doi.org/10.1002/nme.1620150914.

[21]   F. V Antunes, D. Camas, L. Correia, and R. Branco, "Finite element meshes for optimal modelling of plasticity induced crack closure," *Eng. Fract. Mech.*, vol. 142, pp. 184–200, 2015, doi: https://doi.org/10.1016/j.engfracmech.2015.06.007.

[22]   L. P. Borrego, J. M. Ferreira, J. M. Pinho da Cruz, and J. M. Costa, "Evaluation of overload effects on fatigue crack growth and closure," *Eng. Fract. Mech.*, vol. 70, no. 11, pp. 1379–1397, 2003, doi: https://doi.org/10.1016/S0013-7944(02)00119-4.

[23]   M. F. Borges, F. V Antunes, B. Moreno, P. Prates, D. Camas, and D. M. Neto, "Fatigue crack propagation analysis in 2024-T351 aluminium alloy using nonlinear parameters," *Int. J. Fatigue*, no. Apr, 2021.

[24]   F. F. Ferreira, D. M. Neto, J. S. Jesus, P. A. Prates, and F. V Antunes, "Numerical Prediction of the Fatigue Crack Growth Rate in SLM Ti-6Al-4V Based on Crack Tip Plastic Strain," *Metals (Basel).*, vol. 10, no. 9, 2020, doi: 10.3390/met10091133.